HHS Public Access

Author manuscript

J Am Chem Soc. Author manuscript; available in PMC 2024 July 25.

Published in final edited form as:

J Am Chem Soc. 2024 July 24; 146(29): 20349–20356. doi:10.1021/jacs.4c05881.

Cooperative Phosphine-Photoredox Catalysis Enables N–H Activation of Azoles for Intermolecular Olefin Hydroamination

Kassandra Sedillo[1], **Flora Fan**[2], **Robert R. Knowles**[1], **Abigail G. Doyle**[2]

[1]Department of Chemistry, Princeton University, Princeton, New Jersey 08544, United States

[2]Department of Chemistry and Biochemistry, University of California, Los Angeles, California 90095, United States

Abstract

Catalytic intermolecular olefin hydroamination is an enabling synthetic strategy that offers direct and atom-economical access to a variety of nitrogen-containing compounds from abundant feedstocks. However, despite numerous advances in catalyst design and reaction development, hydroamination of N–H azoles with unactivated olefins remains an unsolved problem in synthesis. We report a dual phosphine and photoredox catalytic protocol for the hydroamination of numerous structurally diverse and medicinally relevant N–H azoles with unactivated olefins. Hydroamination proceeds with high anti-Markovnikov regioselectivity and *N*-site selectivity. The mild conditions and high functional group tolerance of the reaction permit the rapid construction of molecular complexity and late-stage functionalization of bioactive compounds. N–H bond activation is proposed to proceed via polar addition of the N–H heterocycle to a phosphine radical cation, followed by P–N α-scission from a phosphoranyl radical intermediate. Reactivity and *N*-site selectivity are classified by heterocycle N–H BDFE and nitrogen-centered radical (NCR) spin density, respectively, which can serve as a useful predictive aid in extending the reaction to unseen azoles.

Graphical Abstract

Corresponding Authors: **Abigail G. Doyle** – Department of Chemistry and Biochemistry, University of California, Los Angeles, California 90095, United States; agdoyle@chem.ucla.edu, **Robert R. Knowles** – Department of Chemistry, Princeton University, Princeton, New Jersey 08544, United States; rknowles@princeton.edu.

The authors declare no competing financial interest.

ASSOCIATED CONTENT

Supporting Information

The Supporting Information is available free of charge on the ACS Publications website.

Experimental procedures, experimental data, code, and characterization and spectral data for new compounds (PDF).

Data from quantum mechanics calculations (.xslx)

Accession Codes

CCDC 2341285 contains the supplementary crystallographic data for this paper. These data can be obtained free of charge via www.ccdc.cam.ac.uk/data_request/cif, or by emailing data_request@ccdc.cam.ac.uk, or by contacting The Cambridge Crystallographic Data Centre, 12 Union Road, Cambridge CB2 1EZ, UK; fax: +44 1223 336033.

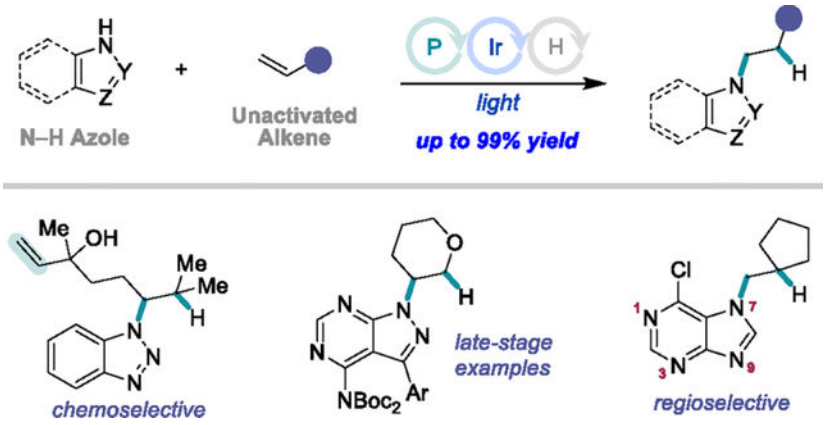

Keywords

phosphine catalysis; photoredox catalysis; phosphoranyl radical; hydroamination; azoles

INTRODUCTION

The prevalence of nitrogen heterocycles in natural products, pharmaceuticals, and agrochemicals, has fueled a demand for new methodologies that enable their synthesis and diversification.[1–3] While strategies for *N*-arylation of azoles have been extensively developed, fewer modern catalytic methods exist for *N*-alkylation.[4–7] *N*-Aryl azoles are much more common in pharmaceuticals than *N*-alkyl azoles, which may in part be due to the challenge of achieving mild, efficient, and selective azole alkylation. Regardless, given the growing recognition of the importance of C(sp^3) incorporation in new drugs and agrochemicals,[8–10] the development of broadly applicable methods for *N*-alkylation of N–H azoles represents an important goal.

Well-established approaches for N–C(sp^3) bond formation rely on nucleophilic addition of *N*-centered nucleophiles to an electrophile, such as an alkyl (pseudo)halide or carbonyl compound.[11] However, the low nucleophilicity of N–H azoles often necessitates harsh reaction conditions that are incompatible with incorporation of secondary or tertiary aliphatic substituents and are not applicable in complex settings.[12, 13] Recently, photo- and electrochemical methods have emerged as a powerful alternative approach toward azole *N*-alkylation with a diverse set of electrophiles, providing regioselective product formation under mild conditions.[14–16] These strategies typically rely on the formation of *C*-centered radicals or carbocation intermediates from abundant precursors, such as alkyl halides, alkyl carboxylic acids, alkanes, or redox-active esters (Figure 1A). Even with the development of these important synthetic technologies, there is a need for mechanistically distinct approaches that show tolerance across many medicinally relevant heterocycle classes, enable access to products with complementary chemo- and regioselectivity, and engage different classes of feedstocks.

Intermolecular olefin hydroamination represents an attractive strategy for the alkylation of N–H azoles due to its atom-economy and the availability of olefin feedstocks.[17] However,

because most N–H substrates and olefins are nucleophilic, a catalyst is necessary to mediate their reaction.[18] Numerous advances have been made in transition metal-catalyzed intermolecular hydroamination, but only a single report describes the reaction of an N–H azole class, N–H indoles, with unactivated olefins.[19] Although remarkable, the scope is limited to indoles and only accommodates terminal olefins with Markovnikov selectivity. Similarly, important progress has been made in photocatalytic hydroamination with heterocycles via nucleophilic addition to an olefin radical cation, but no reports demonstrate formation of *N*-alkylazole products using unactivated olefins (Figure 1B).[20] A complementary approach involves the formation of electrophilic *N*-centered radicals (NCRs), since their reaction with unactivated olefins is polarity matched.[21, 22] The Knowles group, amongst others, has contributed new photocatalytic approaches to N–H activation of a variety of classes of amines and (sulfon)amides.[23] However, N–H azoles have not been reported. Recent work by the groups of Zhang[24] and Chen[25] have demonstrated the feasibility of alkene hydroamination via heterocylic NCRs using *N*-functionalized azoles, such as *N*-pyridinium salts and hydroxybenzotriazoles, respectively. Thus, identification of a mild and general strategy for N–H bond activation of azoles could prove highly enabling in the development of this and numerous other reactions that deliver medicinally relevant heterocyclic products.

The Doyle group recently reported a phosphine-photoredox catalytic platform that activates N–H bonds of primary sulfonamides (BDFE ~105 kcal/mol) and delivers NCRs via α-scission of the P–N bond of a phosphoranyl radical intermediate.[26] We questioned whether this strategy could be extended to N–H azoles and selected to evaluate substrates with a wide range of N–H BDFEs (68−117 kcal/mol) (Figure 1C). Nevertheless, the ambident reactivity of many N–H azoles and their low nucleophilicity presents a potential challenge to their use under this protocol; nucleophilic addition to a phosphine radical cation affords the phosphoranyl radical intermediate and we had previously found that this step was sensitive to the steric hindrance of sulfonamide substrates, where primary sulfonamides reacted selectively over secondary sulfonamides. Despite this concern, we anticipated that the modularity of the dual catalytic system would offer an opportunity to identify an efficient protocol. Here we demonstrate a general method for *N*-alkylation of a variety of azoles by intermolecular anti-Markovnikov hydroamination of unactivated olefins using the combination of phosphine and photoredox catalysts under visible light irradiation (Figure 1D).

RESULTS AND DISCUSSION

Reaction Development.

We commenced reaction optimization using benzimidazole (**1**) and methylenecyclopentane as model substrates. On the basis of our previously disclosed sulfonamide hydroamidation, we first explored the use of tricyclohexylphosphine (PCy_3), $[Ir(dF(Me)ppy)_2(dtbbpy)]PF_6$ ($^*Ir^{III}/Ir^{II}$ = +0.97 V vs SCE in MeCN), and tri*iso*propylbenzenethiol (TRIP-SH) as catalysts for the transformation. Hydroamination product **2** was formed in 55% yield using 2.5 mol% PCy_3, 2 mol% photocatalyst, and 10 mol% TRIP-SH with a 427 nm lamp (34 W) at 50% intensity (Table 1, entry 1). While an increase in product yield was observed when the

phosphine loading was increased from 2.5 to 10 mol%, increasing the loading further led to a decrease in product formation, presumably due to competitive addition of phosphine to the phosphine radical cation (Table 1, entries 2–5). Alternative commercially available trialkylphosphines also provided *N*-alkylated product in good yield (Table 1, entries 6–7). Although dicyclohexylphenylphosphine (PCy_2Ph) afforded **2** in 58% yield, phosphines with more complex aryl substituents, such as BrettPhos and DavePhos, were essentially unreactive (Table 1, entries 8–10). Moreover, triphenylphosphine (PPh_3) formed product in only 8% yield (Table 1, entry 11). Examining photocatalysts with various excited-state oxidation potentials demonstrated that **PC 1** is optimal for this method, presumably because it delivers a strong driving force for the generation of the phosphine radical cation (Table 1, entries 12–13). Product formation was improved to 82% yield when the light intensity of the 427 nm lamp (34 W) was increased from 50% to 100% (Table 1, entry 14). Finally, control experiments indicated that no product formation occurs in the absence of phosphine catalyst, photocatalyst, hydrogen atom transfer (HAT) catalyst, or irradiation (Table 1, entries 15–18).

Azole Scope.

With the optimized protocol in hand, we investigated the scope of *N*-alkylation with various azole classes. Notably, we found that for certain N–H azoles, use of 20 mol% PPh_3 instead of PCy_3 under otherwise identical reaction conditions was necessary to achieve efficient hydroamination (See SI for details). Moreover, results employing PPh_3 as the catalyst were reproducible using Schlenk technique, as indicated in Scheme 1. We first examined substituted benzimidazoles and discovered that substituents at numerous positions around the ring are compatible with the method. A 93% yield of **3** was obtained using 2-chlorobenzimidazole, a common precursor for the synthesis of antihistaminic norastemizole. Fluorinated substrates substituted at the 4- and 5-positions, such as 4-trifluoromethylbenzimidazole and 5-fluoro-benzimidazole, provided *N*-alkylated products **4** and **5** in 99 and 42% yield, respectively. Moreover, 4- and 5-azabenzimidazoles have been shown to have medicinal significance due to their biophysical and biochemical properties among a multitude of diseases.[27] We found that these N–H azoles delivered products **6** and **7** in excellent yield. Unfortunately, low *N*-site selectivity is observed for the hydroamination of unsymmetric benzimidazoles. However, we found that the regioisomers are separable by chromatography and thus offer an opportunity to access a library of *N*-alkylated benzimidazoles from readily available precursors. With the success of benzimidazoles, we set out to explore the compatibility of our method with other privileged N–H azoles.

Purines are the most abundant nitrogenous azoles in nature, serving as constituents of nucleic acids.[28] Current approaches to N^7-alkylated purines rely on laborious synthetic manipulations or methods that provide the N^9-alkylated isomer as the major product.[29, 30] Therefore, we were excited to find that purines were not only competent substrates for the phosphine/photoredox hydroamination protocol, but they also delivered high N^7-alkylation selectivity as confirmed by X-ray structure determination. For example, readily available 6-chloropurine afforded **8** in 70% yield with nearly exclusive N^7 selectivity (>20:1 N^7:N^9). Derivatives of adenine, guanine, and 6-mercaptopurine also afforded products in high yields (**9**–**11**).

As triazoles, pyrazoles, and indazoles have been frequently employed in medicinal chemistry, we investigated these N–H azole classes as well. Although these azoles tend to be plagued with ambident reactivity, where multiple *N*- and *C*- atoms are reactive, the hydroamination reaction of these nucleophiles delivered exclusive N^1-alkylated isomers. Unsubstituted 1,2,4-triazole and 3-phenyltriazole were converted to products **12** and **13** in high yields. Moreover, pyrazoles bearing phenyl (**14**), carbamate (**15**), and ester (**16**–**17**) substituents were well-tolerated. Unsubstituted indazole (**18**) and 3-substituted indazoles **19** and **20** also underwent hydroamination in good yields. Finally, as a testament to the mild conditions and complementary functional group tolerance of this method compared to polar chemistry and transition metal catalysis for *N*-alkylation, we found that an aldehyde-functional group was tolerated, delivering indazole derivative **21**, albeit in 20% yield.

We then turned our attention to 7-azaindole, a well-established motif within various anti-cancer agents, and benzotriazoles, which are also important building blocks for drug discovery.[31] Both heterocycles are competent substrates under the hydroamination conditions. 7-azaindoles deliver exclusive *N*- rather than *C*-alkylated products **22** and **23**. Benzotriazole was found to react with 2-methylheptene to provide **24** in 92% yield with exclusive N^1-alkylation. However, modest N^1 and N^3 selectivity was observed when using substituted benzotriazoles as substrates (**25** and **26**). Additionally, 5-pinacol boronic ester-benzotriazole formed product **27** in 30% yield, demonstrating compatibility of labile functionality to the reaction conditions and delivering a product with a modular handle for further diversification. Finally, to highlight the versatility of the method for late-stage synthesis, we tested *N*-alkylation of the Boc-protected heterocyclic core of ibrutinib. The hydroamination protocol could enable the generation of a library of N^1-alkylated ibrutinib derivatives at a late-stage as highlighted by the synthesis of **28,** which was formed in 95% yield, and features an N^1-tetrahydropyran whereas ibrutinib possesses an N^1-piperidine. It was found that protecting the amino group on the ibrutinib fragment is necessary for efficient alkylation of the azole due to functional group incompatibility of the free aniline (See SI for details).

Olefin Scope.

Next, we evaluated the scope of the olefin partner using benzotriazole,[32] a useful heterocyclic building block with applications in pharmaceuticals,[33] corrosion inhibitors,[34] materials,[35] and supramolecular ligands (Scheme 2).[36] Both linear and cyclic 1,1-disubstituted olefins are highly reactive in this system providing **24** and **29** in 92% and 96% yield, respectively. Cyclohexene and cyclooctene afforded **30** and **31**, demonstrating that internal olefins of various ring sizes are competent coupling partners. Additionally, cyclic and acyclic trisubstituted olefins afforded the desired hydroamination products **32**–**34** in 78–95% yield and tetramethylethylene reacted to give **35** in excellent yield. Notably, **34** was obtained as separable regioisomers, delivering anti-Markovnikov and Markovnikov products in a 9:1 ratio. DFT computations were consistent with the experimental ratio and support that the product selectivity is dependent on the rate of NCR addition to the olefin (See SI for details).

We also observed that a wide variety of functional groups were well-tolerated on the olefin partner, including carbamates (**36**), lactams (**37**), acyclic (**38**) and cyclic ethers (**39**), as well as esters (**40**) and unprotected primary alcohols (**41**). (±)-Linalool underwent regioselective hydroamination favoring reaction at the more electron-rich trisubstituted olefin in the presence of the monosubstituted olefin (**42**). Nootkatone, an insect repellant, also reacts in good yield with exclusive addition of benzotriazole to the 1,1-disubstituted olefin over the α,β-unsaturated ketone (**43**). Although this reaction is applicable to a variety of alkene partners, monosubstituted terminal aliphatic and styrenyl olefins represent limitations of the current protocol. Overall, this method offers a new strategy to access a diverse array of valuable products from N–H azoles and unactivated or electron-rich olefins.

Mechanistic Investigation.

On the basis of our prior mechanistic work on sulfonamide hydroamination and the similarity in reaction conditions between the N–H azole and sulfonamide hydroaminations, we envisioned the catalytic cycle depicted in Figure 2A. Blue light irradiation of the iridium photocatalyst, followed by single-electron transfer (SET) between the excited photocatalyst and phosphine **A** delivers a reduced photocatalyst and phosphine radical cation **B**. Subsequent nucleophilic addition of azole **D** would form phosphoranyl radical intermediate **C**. α-Scission of the P–N bond of **C** regenerates the phosphine catalyst **A** and liberates an *N*-centered radical **E**. C–N bond formation be tween **E** the olefin partner furnishes a *C*-centered radical **F** that undergoes HAT with the thiol catalyst. SET of thiyl radical **I** with the reduced photocatalyst, followed by proton transfer (PT) regenerates the HAT catalyst and completes the catalytic cycle.

In addition to phosphorus-mediated α-scission, we considered two other mechanistic scenarios: 1) direct oxidation of the N–H azole substrate by the excited photocatalyst and 2) N–H activation via a proton-coupled electron transfer (PCET) pathway. We conducted Stern–Volmer studies to assess both pathways using the photocatalyst and four azole classes: benzimidazole, benzotriazole, indazole, and 7-azaindole. In all cases, we observed that the photocatalyst is not quenched by the azole substrate alone nor when combined with the corresponding phosphine at a constant concentration, as showcased for benzimidazole (Figure 2B, *left*). In contrast, the excited photocatalyst undergoes concentration-dependent quenching by PCy_3 and PPh_3, which is consistent with the formation of a phosphine radical cation, a key intermediate in the proposed mechanism (Figure 2B, *right*). Altogether, the studies support the proposed catalytic cycle.

During the course of our scope studies, we collected reactivity data on the hydroamination of cyclohexene or methylene cyclopentane with 105 substituted N–H azoles, some of which showed limited or no reactivity under the standard reaction conditions (see SI for full list). We therefore sought to build a model that could identify unreactive substrates ahead of experimental evaluation and offer mechanistic insight into the factors governing reactivity and selectivity. We posited nucleophilicity of the azole could dictate the rate of addition to the phosphine radical cation and pK_a may influence the deprotonation step necessary to form the phosphoranyl radical intermediate. Additionally, the N–H BDFE relates to the thermodynamics of the α-scission step and the *N*-atom charge could be responsible for the

rate of olefin addition to generate the C–N bond.[37] To investigate these hypotheses, we used DFT computations on the N–H azoles to extract molecular and atomic properties such as pK_a, atomic charge, and N–H BDFE.

After removing substrates bearing incompatible functional groups (amides, anilines, bromides, and iodides), we observed a reactivity threshold with the BDFE of the N–H azole, where substrates with BDFEs below ~90 kcal/mol are unreactive (Figure 3). This threshold explains the inefficient product formation from some common azoles, such as carbazole and indole (Figure 3B). Due to the relation of N–H BDFE values and NCR stability, it is likely that azoles with BDFEs below the threshold have high concentrations of the NCR relative to phosphoranyl radical; reversible or slow addition of these NCRs to the alkene could lead to unproductive back-electron transfer (BET) or other decomposition pathways. One false negative is found in this classification. This substrate, 3-phenylindazole, is structurally similar to other reactive azoles and possesses stronger concentration of the HOMO and spin density on nitrogen, which may make up for the low BDFE. Conversely, the false positive examples in the classification have HOMOs that are not concentrated on the *N*-atom expected to undergo alkylation (See SI for details). Thus, while it is likely a combination of multiple factors that lead to productive reactivity, this simple BDFE classification can serve as a predictive tool for pre-screening N–H azoles that are likely to be effective under the catalytic protocol.

Finally, we questioned the origin of regioselectivity for ambident azoles. We posited that high concentration of spin density relates to the favorable site of reactivity. Indeed, NCR spin density calculations are consistent with this proposal, wherein the major isomer of *N*-alkylation corresponds to the *N*-atom with highest spin density in the NCR. However, differences in spin density do not capture the magnitude of the experimental selectivity observed (Figure 4) (See SI for details).

CONCLUSION

In conclusion, we have showcased the application of phosphine-photoredox catalysis to the generation of *N*-centered radicals from a variety of azole classes via activation of N–H bonds. The catalytic protocol was applied to the chemo- and regioselective synthesis of valuable *N*-alkylated azoles via the intermolecular anti-Markovnikov hydroamination of unactivated olefins. Mechanistic studies support the azole radical generation proceeds via α-scission of a phosphoranyl radical intermediate. A threshold was identified for reactivity which correlates well with N–H BDFEs. Moreover, regioselectivity corresponds with NCR spin density. This study expands the synthetic utility of the phosphoranyl radical α-scission activation mode.

Supplementary Material

Refer to Web version on PubMed Central for supplementary material.

ACKNOWLEDGMENT

We thank Dr. Jackson Deobald and Cesar Nicolas Prieto Küllmer for intellectually engaging and creative discussions toward this research. We also thank Judah Raab for solving the X-Ray crystal structure.

Funding Sources

Financial support for this work was provided by the NIGMS (R35GM126986 to AGD and R35-GM134893 to RRK). These studies were also supported by shared instrumentation grants from the National Science Foundation (CHE-1048804), NIH Office of Research Infrastructure Programs (S10OD028644), and used computational and storage services associated with the Hoffman2 Shared Cluster provided by UCLA Institute for Digital Research and Education's Research Technology Group.

REFERENCES

(1). Froidevaux V; Negrell C; Caillol S; Pascault JP; Boutevin B Biobased Amines: From Synthesis to Polymers; Present and Future. Chem Rev 2016, 116 (22), 14181–14224. DOI: 10.1021/acs.chemrev.6b00486 [PubMed: 27809503]

(2). Vitaku E; Smith DT; Njardarson JT Analysis of the structural diversity, substitution patterns, and frequency of nitrogen heterocycles among U.S. FDA approved pharmaceuticals. J Med Chem 2014, 57 (24), 10257–10274. DOI: 10.1021/jm501100b [PubMed: 25255204]

(3). Dugger RWR, Brown Ripin JA, Surve D. H. y of GMP Bulk Reactions Run in a Research Facility between 1985 and 2002. ORPD 2005, 9 (3), 253–258. DOI: 10.1021/op050021j.

(4). Ravindar L; Hasbullah SA; Hassan NI; Qin HL Cross-Coupling of C–H and N–H Bonds: A Hydrogen Evolution Strategy for the Construction of C–N Bonds. European Journal of Organic Chemistry 2022, 2022 (31). DOI: 10.1002/ejoc.202200596.

(5). Trowbridge A; Walton SM; Gaunt MJ New Strategies for the Transition-Metal Catalyzed Synthesis of Aliphatic Amines. Chem Rev 2020, 120 (5), 2613–2692. DOI: 10.1021/acs.chemrev.9b00462 [PubMed: 32064858]

(6). Hazari N; Melvin PR; Beromi MM Well-defined nickel and palladium precatalysts for cross-coupling. Nat Rev Chem 2017, 1. DOI: 10.1038/s41570-017-0025

(7). Ruiz-Castillo P; Buchwald SL Applications of Palladium-Catalyzed C-N Cross-Coupling Reactions. Chem Rev 2016, 116 (19), 12564–12649. DOI: 10.1021/acs.chemrev.6b00512 [PubMed: 27689804]

(8). Jeschke P Current status of chirality in agrochemicals. Pest Manag Sci 2018, 74 (11), 2389–2404. DOI: 10.1002/ps.5052 [PubMed: 29704299]

(9). Foley DJ; Craven PGE; Collins PM; Doveston RG; Aimon A; Talon R; Churcher I; von Delft F; Marsden SP; Nelson A Synthesis and Demonstration of the Biological Relevance of sp(3)-rich Scaffolds Distantly Related to Natural Product Frameworks. Chemistry 2017, 23 (60), 15227–15232. DOI: 10.1002/chem.201704169 [PubMed: 28983993]

(10). Lovering F; Bikker J; Humblet C Escape from flatland: increasing saturation as an approach to improving clinical success. J Med Chem 2009, 52 (21), 6752–6756. DOI: 10.1021/jm901241e [PubMed: 19827778]

(11). Trost BMF, I. Comprehensive Organic Synthesis: Reduction; Elsevier Science & Technology Books, 1991.

(12). Brown DG; Bostrom J Analysis of Past and Present Synthetic Methodologies on Medicinal Chemistry: Where Have All the New Reactions Gone? J Med Chem 2016, 59 (10), 4443–4458. DOI: 10.1021/acs.jmedchem.5b01409 [PubMed: 26571338]

(13). Constable DJC; Dunn PJ; Hayler JD; Humphrey GR; Leazer JJL; Linderman RJ; Lorenz K; Manley J; Pearlman BA; Wells A; et al. Key green chemistry research areas—a perspective from pharmaceutical manufacturers. Green Chem. 2007, 9 (5), 411–420. DOI: 10.1039/b703488c

(14). Yuan Y; Yang J; Lei A Recent advances in electrochemical oxidative cross-coupling with hydrogen evolution involving radicals. Chem Soc Rev 2021, 50 (18), 10058–10086. DOI: 10.1039/d1cs00150g [PubMed: 34369504]

(15). Rivas M; Palchykov V; Jia X; Gevorgyan V Recent advances in visible light-induced C(sp (3))-N bond formation. Nat Rev Chem 2022, 6 (8), 544–561. DOI: 10.1038/s41570-022-00403-8 [PubMed: 37034136]

(16). Talekar SS; Dutta S; Mane MV; Maity B Visible Light-Induced Photoredox and Copper-Catalyzed C–N Cross-Coupling: A Mechanistic Perspective. European Journal of Organic Chemistry 2024, 27 (11). DOI: 10.1002/ejoc.202301312.

(17). Ma S; Hartwig JF Progression of Hydroamination Catalyzed by Late Transition-Metal Complexes from Activated to Unactivated Alkenes. Acc Chem Res 2023, 56 (12), 1565–1577. DOI: 10.1021/acs.accounts.3c00141 [PubMed: 37272995]

(18). Huang L; Arndt M; Goossen K; Heydt H; Goossen LJ Late transition metal-catalyzed hydroamination and hydroamidation. Chem Rev 2015, 115 (7), 2596–2697. DOI: 10.1021/cr300389u [PubMed: 25721762]

(19). Sevov CS; Zhou JS; Hartwig JF Iridium-catalyzed, intermolecular hydroamination of unactivated alkenes with indoles. J Am Chem Soc 2014, 136 (8), 3200–3207. DOI: 10.1021/ja412116d [PubMed: 24483848]

(20). Luo MJ; Xiao Q; Li JH Electro-/photocatalytic alkene-derived radical cation chemistry: recent advances in synthetic applications. Chem Soc Rev 2022, 51 (16), 7206–7237. DOI: 10.1039/d2cs00013j [PubMed: 35880555]

(21). Kwon K; Simons RT; Nandakumar M; Roizen JL Strategies to Generate Nitrogen-centered Radicals That May Rely on Photoredox Catalysis: Development in Reaction Methodology and Applications in Organic Synthesis. Chem Rev 2022, 122 (2), 2353–2428. DOI: 10.1021/acs.chemrev.1c00444 [PubMed: 34623809]

(22). Pratley C; Fenner S; Murphy JA Nitrogen-Centered Radicals in Functionalization of sp(2) Systems: Generation, Reactivity, and Applications in Synthesis. Chem Rev 2022, 122 (9), 8181–8260. DOI: 10.1021/acs.chemrev.1c00831 [PubMed: 35285636]

(23). Geunes EP; Meinhardt JM; Wu EJ; Knowles RR Photocatalytic Anti-Markovnikov Hydroamination of Alkenes with Primary Heteroaryl Amines. J Am Chem Soc 2023, 145 (40), 21738–21744. DOI: 10.1021/jacs.3c08428 [PubMed: 37787499]

(24). Wang L; Shi M; Chen X; Su N; Luo W; Zhang X Generation of Aromatic N-Heterocyclic Radicals for Functionalization of Unactivated Alkenes. Angew Chem Int Ed Engl 2023, 62 (52), e202314312. DOI: 10.1002/anie.202314312 [PubMed: 37946626]

(25). Zhu F; Qiao Z; He N; Nong C; He Q; Xi M; Song X; Lin J; Chen J; Jin Y Photoredox Catalyzed Hydroazolylation of Alkenes via Phosphoranyl Radicals. Organic Chemistry Frontiers 2024. DOI: 10.1039/D4QO00233D.

(26). Chinn AJ; Sedillo K; Doyle AG Phosphine/Photoredox Catalyzed Anti-Markovnikov Hydroamination of Olefins with Primary Sulfonamides via alpha-Scission from Phosphoranyl Radicals. J Am Chem Soc 2021, 143 (43), 18331–18338. DOI: 10.1021/jacs.1c09484 [PubMed: 34672192]

(27). Krause MF, Gobis H, K. Pharmacological Potential and Synthetic Appraoches of Imidazo[4,5-*b*]pyridine and Imidazo[4,5-*c*]pyridine Derivatives. Molecules 2017, 22, 399–424. [PubMed: 28273868]

(28). Rosemeyer H The chemodiversity of purine as a constituent of natural products. Chem Biodivers 2004, 1 (3), 361–401. DOI: 10.1002/cbdv.200490033 [PubMed: 17191854]

(29). Kotek V; Chudíková N; Tobrman T; Dvořák D Selective Synthesis of 7-Substituted Purines via 7,8-Dihydropurines. Org Lett 2010, 12 (24), 5724–5727. DOI: 10.1021/ol1025525 [PubMed: 21090632]

(30). Tranova L; Styskala J Study of the N(7) Regioselective Glycosylation of 6-Chloropurine and 2,6-Dichloropurine with Tin and Titanium Tetrachloride. J Org Chem 2021, 86 (19), 13265–13275. DOI: 10.1021/acs.joc.1c01186 [PubMed: 34528791]

(31). Sharman N; Chaudhary AS, Monika. An insight into the structure–activity relationship studies of anticancer medicinal attributes of 7-azaindole derivatives: a review. Future Medicinal Chemistry 2023, 15, 2309–2323. DOI: 10.4155/fmc-2023-0216 [PubMed: 38112047]

(32). Katritzky ARL, X.; Yang JZD, O. V. Properties and Synthetic Utility of *N*-Substituted Benzotriazoles. Chem Rev 1998, 98 (2), 409–548. DOI: 10.1021/cr941170v [PubMed: 11848906]

(33). Suma BV; Natesh NN; Madhavan V Benzotriazole in medicinal chemistry: an overview. J Chem Pharm Res 2011, 3, 375–381

(34). Loi CH, B. F., Linge KL, Joll CA. Development of a solid-phase extraction liquid chromatography tandem mass spectrometry method for benzotriazoles and benzothiazoles in wastewater and recycled water. J Chromatogr A 2013, 1299, 48–57. DOI: 10.1016/j.chroma.2013.04.073 [PubMed: 23768537]

(35). Liu YS, Y. G., Shareef A, Kookana RS. Biodegradation of three selected benzotriazoles in aquifer materials under aerobic and anaerobic conditions. J Contam Hydrol 2013, 151, 131–139. [PubMed: 23777830]

(36). Wang L; Zhao L; Xue R; Lu X; Wen Y; Yang Y Construction of interesting organic supramolecular structures with synthons cooperation in the cocrystals of 1H-benzotriazole and hydroxybenzoic acids. Science China Chemistry 2012, 55 (12), 2515–2522. DOI: 10.1007/s11426-012-4652-4

(37). Parsaee F; Senarathna MC; Kannangara PB; Alexander SN; Arche PDE; Welin ER Radical philicity and its role in selective organic transformations. Nature Reviews Chemistry 2021, 5 (7), 486–499. DOI: 10.1038/s41570-021-00284-3 [PubMed: 37118440]

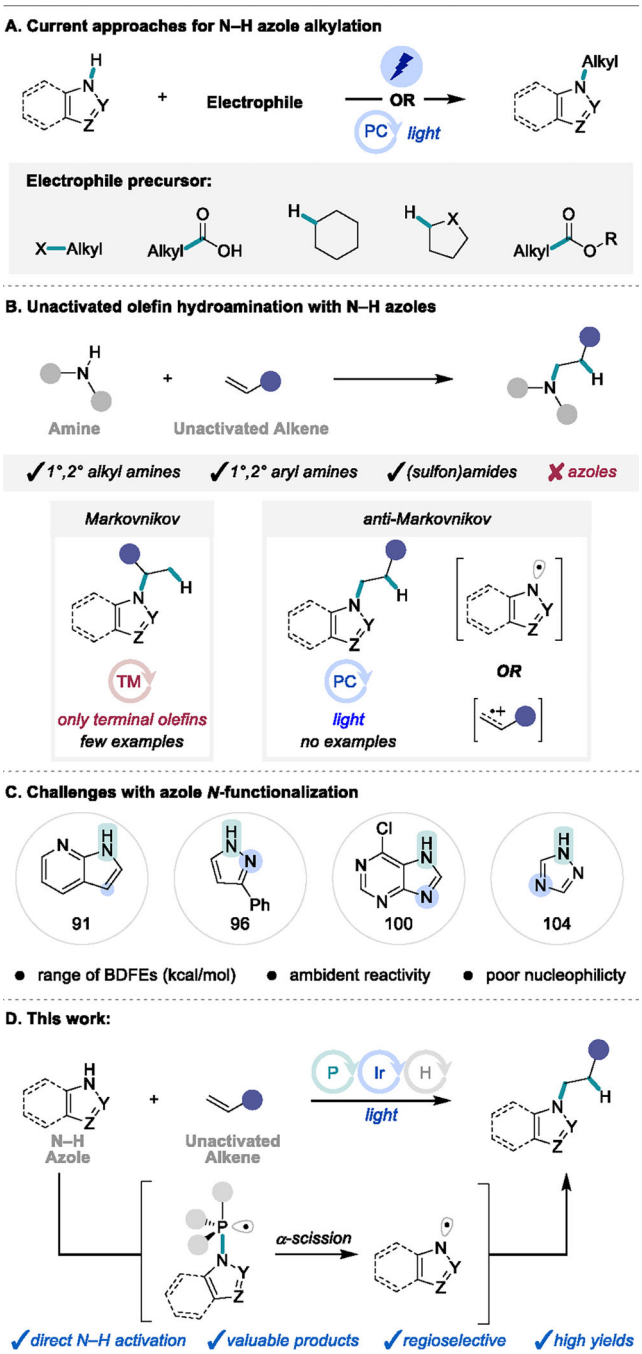

Figure 1. Synthesis of *N*-alkylazoles and limitations.

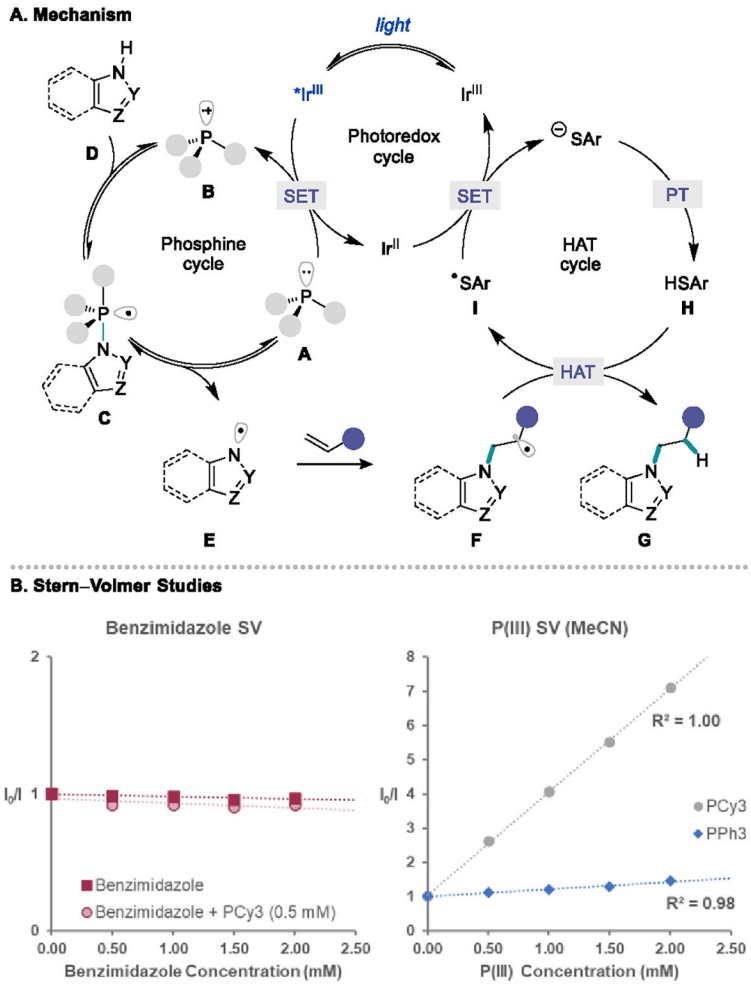

Figure 2.
Mechanism and Stern–Volmer studies.

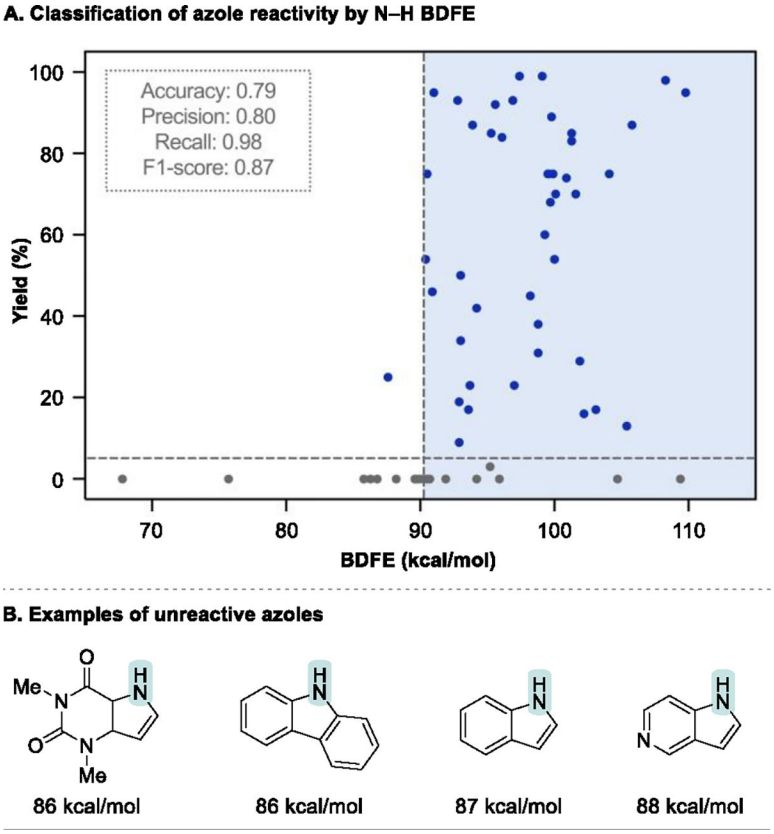

Figure 3.

N–H BDFE corresponds with reactivity. Calculations performed at the (U)M06-2X/Def2-TZVP/SMD(Toluene) level of theory.

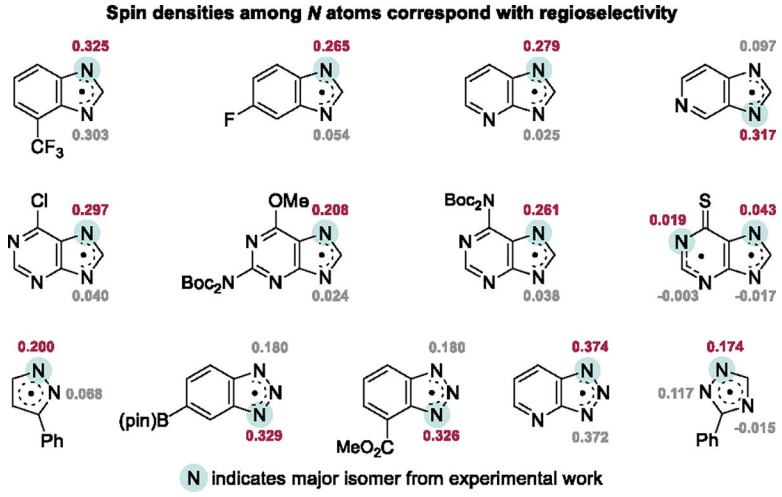

Figure 4.

NCR spin densities and regioselectivity.

Calculations performed at the (U)M06-2X/Def2-TZVP/SMD(Toluene) level of theory.

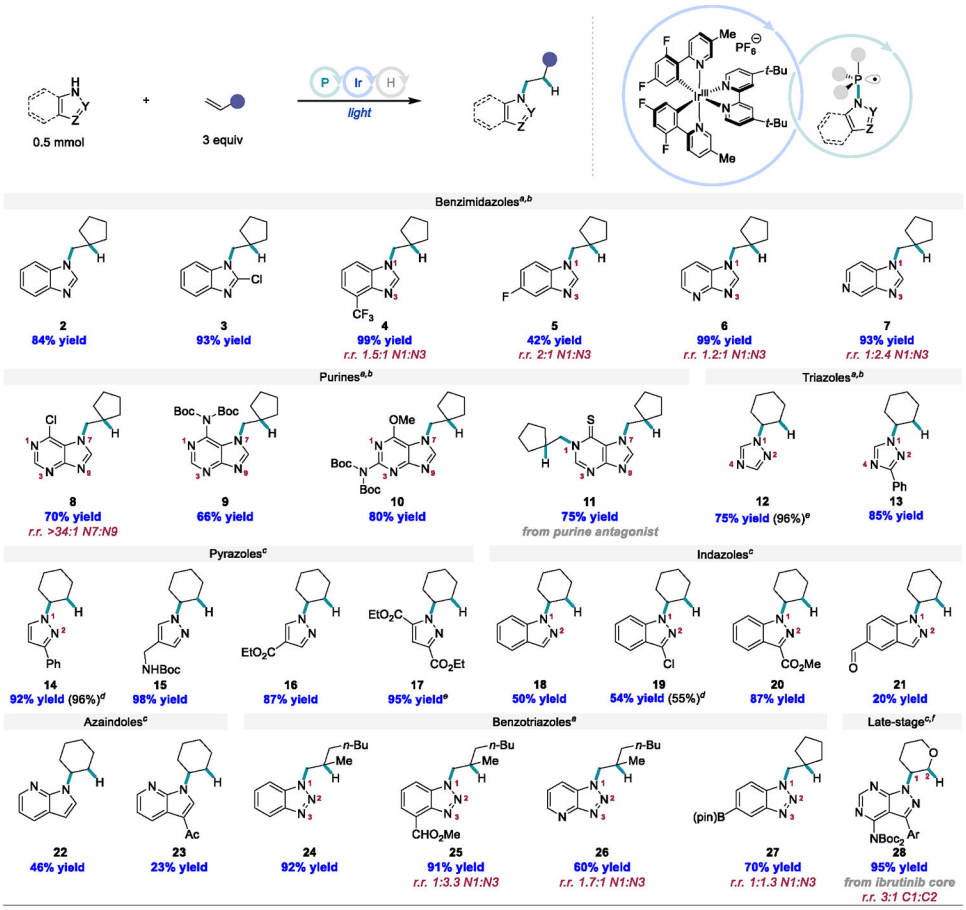

Scheme 1.

Azole Scope.

Reactions were performed on a 0.5 mmol scale reacting 1.0 equiv of azole with 3.0 equiv of olefin using PCy_3 (10 mol%) or PPh_3 (20 mol%) with $[Ir(dF(Me)ppy)_2dtbbpy]PF_6$ (2 mol%), and TRIP-SH (10 mol%) irradiating with a 427 nm lamp at 50% intensity for 16 hours. Isolated yield reported as an average of two runs. [a]PCy_3 was used as phosphine catalyst. [b]427 nm lamp light intensity was set to 100%. [c]PPh_3 was used as the phosphine catalyst. [d]Yields are reflective of reactions set-up using Schlenk technique instead of in a glovebox. [e]Yield determined by ^1H NMR with comparison to internal standard. [f]Ar = *p*-Ph–O–Ph.

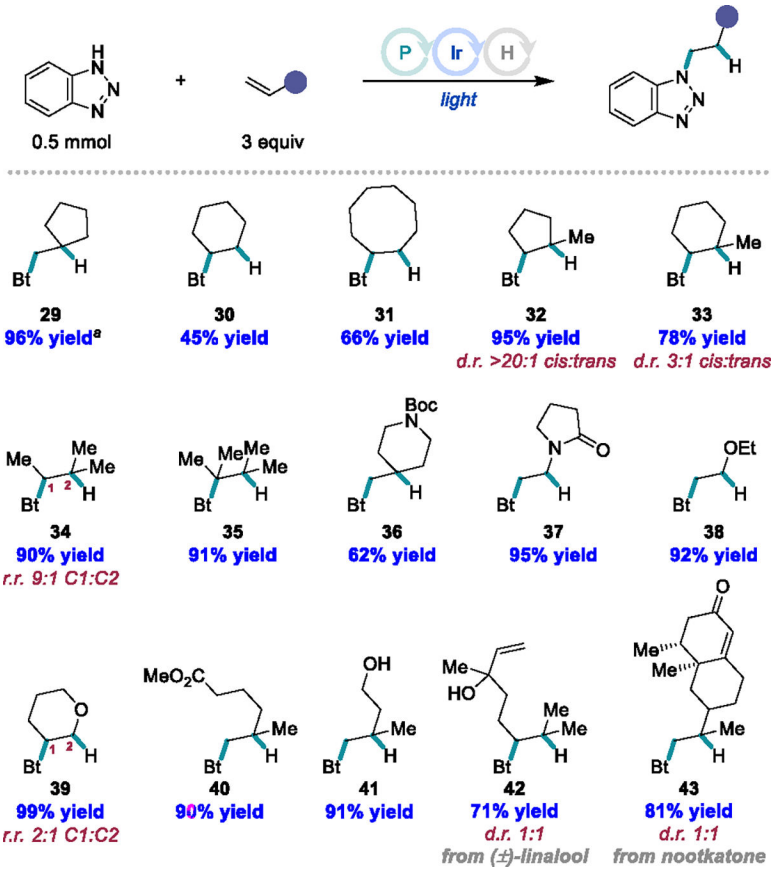

Scheme 2. Olefin Scope.

Reactions were performed on a 0.5 mmol scale reacting 1.0 equiv of benzotriazole with 3.0 equiv of olefin using PCy_3 (10 mol%) with $[Ir(dF(Me)ppy)_2dtbbpy]PF_6$ (2 mol%), and TRIP-SH (10 mol%) irradiating with a 427 nm lamp at 50% intensity for 16 hours. Isolated yield reported as an average of two runs. [a]Yield reproduced after 2 hours using standard conditions.

Table 1.

Optimization Studies

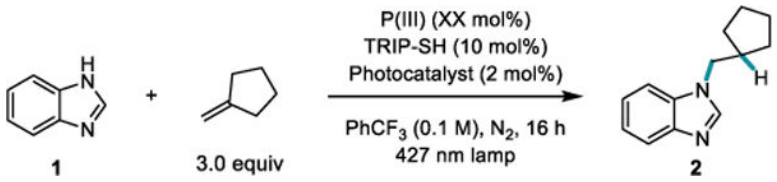

Entry[a]	Phosphine	(P mol%)	Photocatalyst	Yield (%)[b]
1	PCy_3	2.5	PC 1	55
2	PCy_3	5	PC 1	59
3	PCy_3	10	PC 1	71
4	PCy_3	20	PC 1	38
5	PCy_3	40	PC 1	32
6	PAd_2*n*-Bu	10	PC 1	45
7	PAd_3	10	PC 1	45
8	PCy_2Ph	10	PC 1	58
9	BrettPhos	10	PC 1	2
10	DavePhos	10	PC 1	0
11	PPh_3	10	PC 1	8
12	PCy_3	10	PC 2	32
13	PCy_3	10	PC 3	16
14[c]	PCy_3	10	PC 1	**82**

Entry[a]	Deviation from optimal conditions (Entry 3)	Yield (%)[b]
15	No Phosphine	0
16	No Photocatalyst	0
17	No TRIP-SH	0
18	No Light	0

PC 1: $[Ir(dF(Me)ppy)_2(dtbbpy)]PF_6$; $*Ir^{III}/Ir^{II}$ = +0.97 V vs SCE

PC 2: $[Ir(ppy)_2(dtbbpy)]PF_6$; $*Ir^{III}/Ir^{II}$ = +0.66 V vs SCE

PC 3: $[Ir(dF(CF_3)ppy)_2(4,4'\text{-}dCF_3bpy)]PF_6$; $*Ir^{III}/Ir^{II}$ = +1.65 V vs SCE

[a]Reactions were performed on a 0.1 mmol scale with 1.0 equiv of benzimidazole and 3.0 equiv of methylenecyclopentane under irradiation with 427 nm lamp (34 W) at 50% light intensity.

[b]Yield was determined by ^1H NMR spectroscopic analysis against 1,3,5-trimethoxybenzene as an internal standard.

[c]427 nm lamp intensity set to 100% instead of 50%.